IEEE Access
Multidisciplinary | Rapid Review | Open Access Journal

Received May 29, 2018, accepted July 1, 2018, date of publication July 6, 2018, date of current version July 30, 2018.

Digital Object Identifier 10.1109/ACCESS.2018.2853656

Computational Scaling of Shape Similarity That Has Potential for Neuromorphic Implementation

ERNEST GREENE[1], (Member, IEEE), AND JACK MORRISON[2]
[1]Department of Psychology, University of Southern California, Los Angeles, CA 90089, USA
[2]Digital Insight, Somis, CA 93066, USA

Corresponding author: Ernest Greene (egreene@usc.edu)

This work was supported in part by the Neuropsychology Foundation and in part by the Search for Truth Foundation.

ABSTRACT Current methods for encoding and comparing shapes are computationally demanding and are not suitable for image processing in small portable devices. Here, we describe a simple scan encoding method for transcribing shape information into a 1-D summary. Summaries were derived from an inventory of unknown shapes, and these values were used to scale the degree of similarity of pair combinations. The scale values provided a significant level of prediction of human judgments in a match recognition task, suggesting substantial correspondence with human perception of shape similarity. Similarity scores derived with the Procrustes method did not predict human judgments.

INDEX TERMS Shape encoding, shape similarity, retinal encoding, human judgments.

I. INTRODUCTION

"Achieving a better understanding of the brain's visual perceptual mechanisms will be critical for developing robust visual cognitive computing, building compact and energy-efficient intelligent autonomous systems, and establishing new computing architectures for visual perception and understanding of complex scenes." Pengju Ren and associates [1].

In recent decades, there has been increasing interest in what some have called "brain inspired computing," wherein the operations are designed to simulate neuroanatomical and neurophysiological mechanisms [2]. These efforts often draw on computational concepts developed by neuroscientists, with much of the energy being devoted to neural network (connectionist) models for processing of visual images. These models provide not only for recognition of various two- and three-dimensional shapes, but also for mediating translation, size, and rotation invariance [3]–[11].

There is some doubt, however, as to whether connectionist models can deliver computationally efficient image processing. They were designed to simulate interactions among large populations of cortical neurons, with tens of thousands of interconnections and generally requiring many thousands, or tens of thousands, of training trials to achieve invariant shape recognition. It could be useful to focus on simpler systems, such as those which allow fish to navigate the intricacies of coral reefs, recognize predators, and identify members of their own species [12]–[17]. Fish have no cortex, so those visual skills are made possible by circuitry in the retina and/or optic tectum. Providing neuromorphic systems that match the visual skills of fish, in itself, would provide a major advance for robotic vision.

We have additional reasons to urge development of non-connectionist models for shape encoding, based on demonstration of human shape-recognition skills that do not require extensive training trials. Our laboratory has demonstrated that an unknown shape that is seen only once can be identified just a few moments later. It can be recognized even if the location of the shape is translated, or if it is rotated or changed in size [18]. The reported experiments made use of shape outlines that were discretized into strings of dots that we describe as "boundary markers," and the stimuli can be described either as a pattern or as a shape. The shape outlines, i.e., dot sequences, were constructed with arbitrary turns and straight alignments that did not resemble known objects.

Each shape in the inventory was displayed as a brief flash, followed within a few moments by a comparison shape that was "low density," meaning that only some of the boundary markers were displayed. The comparison shape was either a low-density version of the original target shape, or was a low-density version of a different shape, and the respondent was expected to judge whether the second display was a "match" to the original target shape. The judgment process can be described as "match recognition." The data were assessed using bias-correcting methods developed by information

theory, and the judgments were found to be reliably above chance even with large reductions in the density of boundary markers [18]. Further, as stated above, the match judgments were reliably above chance when the location of the comparison shape differed from that of the target shape, or when it was increased in size, or was rotated [18].

It is significant that an unknown shape can be encoded and compared for potential match within moments without any requirement for training trials. It is possible that shape encoding is already beginning within the circuits of the retina, and is passed to other brain areas on the basis of fast and efficient population responses. Greene and Patel [19] suggested that the locations of boundary markers is transcribed into simultaneous ganglion-cell spikes by scanning waves that sweep across the retinal image. The hypothesis was supported by finding that an encoding model that used horizontal and vertical scans to tally the frequency of encounter provided a scale of shape similarity that predicted performance in the match-recognition task described above.

The Greene and Patel [19] experiment provided consistent regression models for each subject and the group data achieved very high statistical significance. Nonetheless, only eight respondents were tested, so it would be good to replicate the findings. Further, it is not clear whether one would get similar results with other methods for scaling shape similarity. Any number of alternative ways for assessing marker locations might yield predictions of performance on the match-recognition task. The underlying concept needs to demonstrate special predictive benefit before being considered by neuromorphic computing engineers.

Toward these ends, the current work has derived scales of shape similarity using Procrustes analysis as well as the scan-encoding method of the earlier report [19]. Procrustes analysis is a statistical method for comparing shape pairs that normalizes distances of boundary markers, e.g., landmarks, relative to the centroids, centers the shapes at their centroids, and then derives the minimum Euclidean distance among all pairs of boundary markers. The method has strong mathematical roots [20]–[23]. The range of applications includes control of tolerance in the manufacture of ''free form'' parts [24], comparison across species in the field of paleontology [25], classification of rock formations in geology [26], and classification of human facial features [27]. It has become a cornerstone method in biology, where it is known as ''geometric morphometrics'' [28]–[33]. Dryden and Mardia [34] provide an overview of the alternative techniques, with examples across a wide range of applications. With a proven record of utility for specifying similarity of diverse shapes, Procrustes analysis should provide a good standard against which to compare other tools for specifying shape similarity.

II. COMPUTATIONAL MODELING

A. SHAPE INVENTORY

The modeling and subsequent test of human judgments used an inventory of 480 amorphous shapes that were designed to minimize similarity to known objects. Each was generated as a single continuous string of dot locations within a 64×64 array, meaning that one could ''step'' from one dot to the next around the boundary with no branches in the path. The shape was displayed as simultaneous brief flashes of light from the specified dots. In the discourse that follows, the light-emitting dots may also be described as ''boundary markers.''

An inventory of 480 shapes provides for 114,960 pairs (combination, choose 2). Three-hundred twenty pairs were chosen for shape-similarity modeling and for perceptual testing, wherein each member of the pair had the same number of boundary markers. This constraint was not needed for the scan encoding method, described below, but simplified the task of assessing similarity for the Procrustes method.

B. DERIVING PROCRUSTES SIMILARITY VALUES FROM SHAPE PAIRS

Procrustes Analysis is a statistical method for specify the similarity of shapes that is designed to assess minimal Euclidean distances among matching points [34]. Full Procrustes analysis adjusts for differentials in orientation and normalizes distances from centroids. If the number of boundary markers is unequal, the method interpolates so that the two shapes being compared will have an equal number of markers. Rotation steps may be required, but were not applied here because respondents were instructed that a matching comparison shape would not be a rotated version of the target shape.

For each pair member, the net distance from the centroid was normalized by dividing each new dot address by the root mean squared distance from the origin. A pair of dots on each shape was chosen and the Euclidian distance between the two normalized addresses was calculated and squared. Proceeding around the boundaries from there, the squared distance for each successive pair was calculated and summed. The square root of that sum provided a candidate Procrustes value. These steps are illustrated in Figure 1.

An optimum Procrustes measure of similarity needs to be the minimum that could be derived by the procedure described above. A single pass through all pairs, starting with an arbitrary choice of starting dots will seldom provide a minimum value. Therefore, the calculation was repeated, starting at the same dot for one shape, choosing a new dot in the second shape for pairing, and then iteratively choosing successive pairs to provide candidate Procrustes values for all pair combinations. The smallest candidate value provided the acceptable Procrustes value for a given shape pair, and these were designated as P-difference values for the inventory of 320 non-matching pairs.

C. DERIVING SCAN SIMILARITY VALUES FROM SHAPE PAIRS

Deriving shape similarity values using scan encoding was based on several basic steps, derived here using only horizontal and vertical scans. For each shape, the following encoding was applied: a) A transcription wave was passed across successive columns of the display, tallying the number of

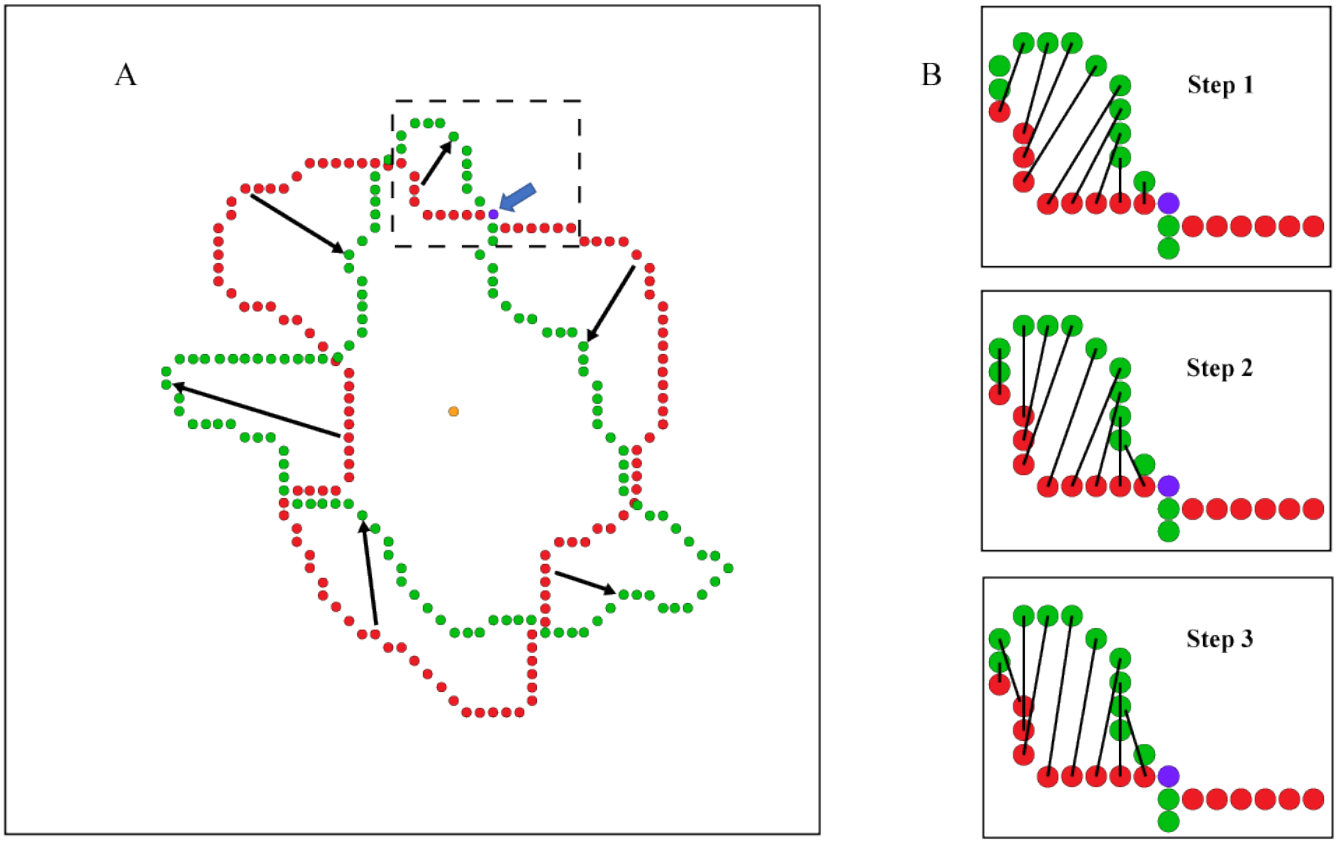

FIGURE 1. Illustration of Procrustes analysis. A. Shapes were normalized for distance and were centered on their centroids (orange), here showing shape 1 in red and shape 69 in green. Distances between pairs of dots were assessed, starting with an arbitrary choice of starting position (purple). Arrows show a few of the spans that would be included in the Procrustes calculation. B. These panels show the first three steps, illustrated with a magnified view of the initial starting position that was chosen. Step 1 sampled the spans that were measured for successive pairs of dots, with this continuing around the boundaries to provided distances for all dot pairs. Step 2 shifted the pairing one position and again provided measures of spans around the full boundary. Step 3 shifted the pairing by two positions and repeated the process. This continued until all possible dot parings were evaluated. The square of the spans were summed, and the square root provided a candidate index for each pairing step. The pairing step yielding the smallest value provided the best Procrustes index for each shape pair. These are designated as P-difference values.

boundary markers in each column. Each column was treated as a bin of a histogram, therefore the count for successive columns provided a complete 64-bin histogram for the horizontal scan. b) A vertical scan provided the count of boundary markers in successive rows, yielding a second 64-bin histogram. c) The two histograms were placed in tandem, providing a 128-bin raw histogram. Note that any columns or rows having zero counts would not contribute to the histograms, so these were trimmed. d) Raw histogram values were re-binned to provide a 20-bin count summary. e) The histograms were normalized to adjust for size differences across pairs. These steps are illustrated in Figure 2. Having derived a summary histogram for each shape, the members of 320 pairs were compared as a simple sum-of-squared-differences calculation across corresponding bin positions. These were designated as S-difference values.

D. RANKING OF DIFFERENCE VALUES TO PROVIDE SHAPE-SIMILARITY SCALES

For purposes of scaling shape similarity, the P-difference values were divided by 100, which coincidentally provided a value range that was approximately the same as the S-difference values.

The left panel of Figure 3 shows a ranking of P-difference values for all pair combinations of the inventory with red tokens, and the corresponding S-difference value at each rank position is shown with a green token. The right panel of Figure 3 shows the reverse. Clearly it is feasible to use the values to derive similarity scales, but the lack of correspondence in the two scales is striking. Correlation of the two scales at corresponding rank positions yielded a correlation of -0.14. In other words, what small correlation exists is negative, so there can be no doubt that the two similarity scales are not assessing common features of the non-matching pairs.

III. JUDGMENT OF SHAPE SIMILARITY WITH A MATCH TASK

A. STIMULUS DISPLAY EQUIPMENT AND CHARACTERISTICS

Shapes were displayed on a custom designed LED board that was fabricated by Digital Insight. The display system consisted of a 64×64 array of AlGaInP LEDs (Super Bright

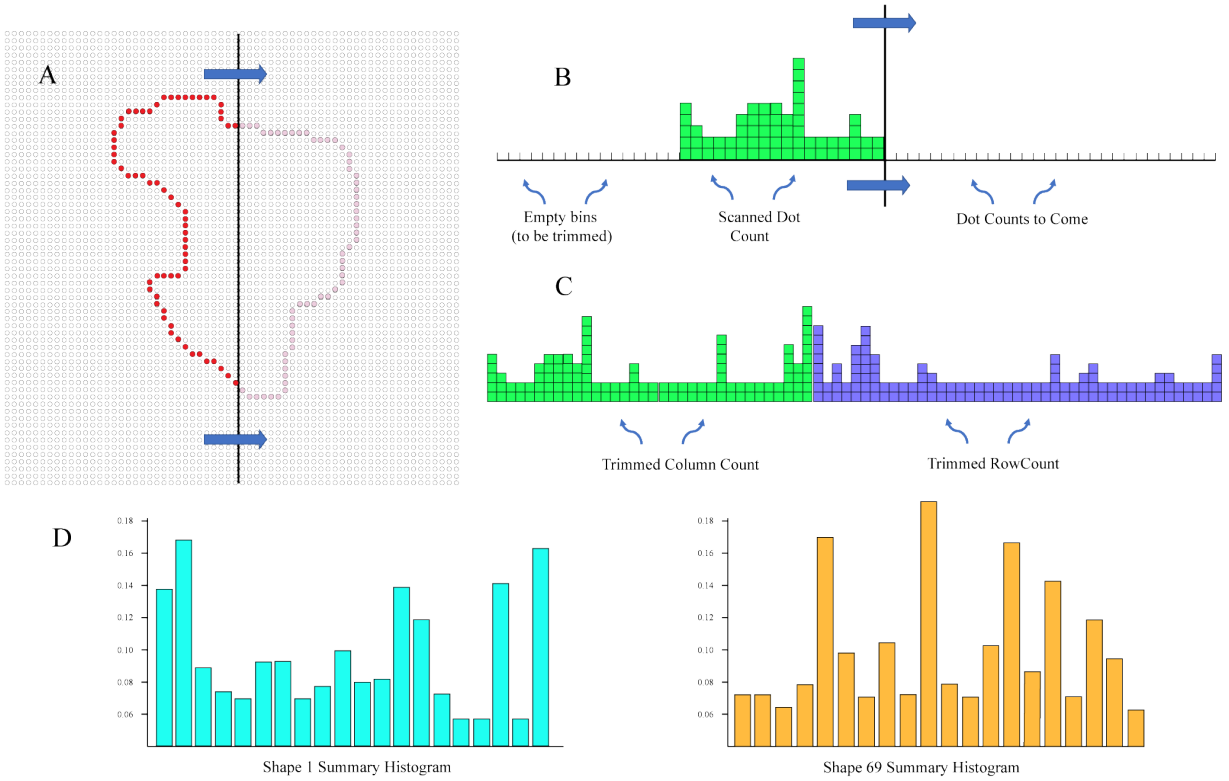

FIGURE 2. A. A polling wave passes across shape 1 transcribing the number of boundary markers into counts that are entered as bin values. B. Bin values reflect the number of successive boundary markers that were encountered by the polling wave. C. Empty bins found by the B step are trimmed and the bin counts for the scan across rows and columns are placed in tandem. D. The raw histogram at C has been re-binned and normalized to provide a summary of shape 1 (cyan). The corresponding histogram for shape 69 is shown to the right (in orange). The two shapes can be compared for similarity by calculating a sum-of-squared differences across corresponding bins (not illustrated).

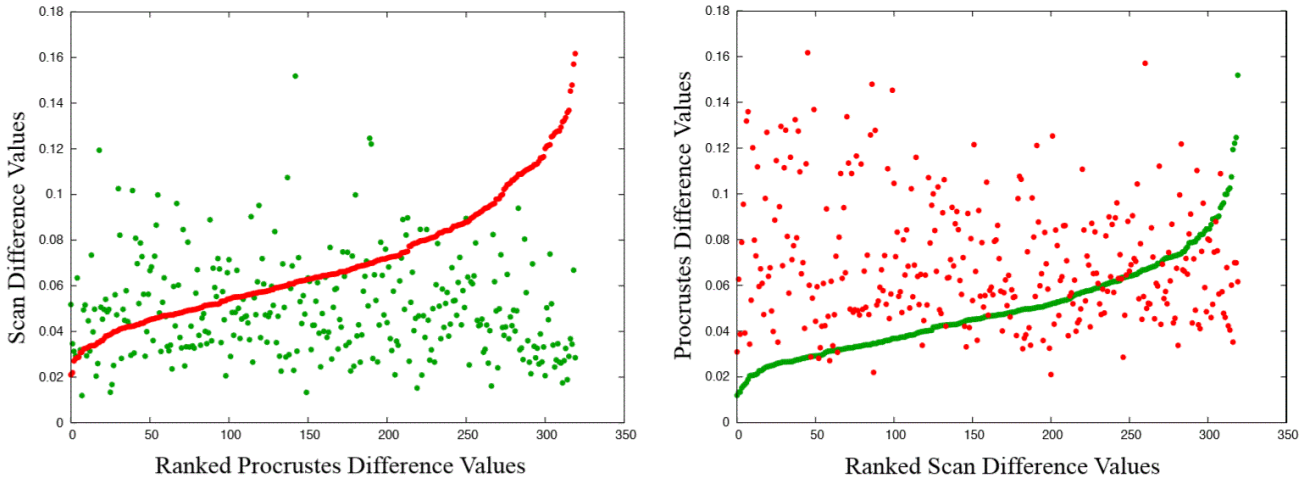

FIGURE 3. Difference values from Procrustes analyses are shown with red tokens and those derived from scan encoding are shown in green. The left panel plots P-difference values ranked by size and the corresponding S-difference value for each pair. The right panel does the reverse. The scattered plot-points in each panel reflect the negative low correlation of the two methods for assessing shape similarity.

part # RL5-R8030) that have peak emission at 630 nm (red). This kind of LED has a typical rise/fall time of 300 ns. The shape of stimulus pulses (flashes) was established using the slowest component of the driving circuit, which provided a rise/fall time estimated to be 70 ns. Diameters and center-to-center spacing of the LEDs were 5 mm and 9.4 mm, respectively, and horizontal and vertical spans of the full array were each 60 cm. Distance from the respondent was 3.5 m, so the corresponding visual angles were 4.92 arc′, 9.23 arc′, and 9.80 arc°, respectively.

A Mac Mini controlled the system using Tcl/tk custom applications written for OS-X. Temporal resolution of all system components was in the nanosecond range. The global timing clock had a minimum period of 1 μs, which provided the limit of experimental control of flash timing.

None of the experimental work involved color comparison, so it is appropriate to report the intensity in radiometric units (μW/sr). Further, physiological studies of photoreceptors with monochromatic or LED light sources often report stimulus energy in radiometric units [35]–[40]. With such narrow-range light sources the responses of red and green cones as a function of intensity are very similar [39].

Intensity was measured using a Thorlabs PM100 radiometer with S120C calibrated silicon photodiode sensor. The calibration process started with power measurements of the display at a distance of one meter, with a single LED turned on and taking readings across a range of LED voltage settings. The reading in μW was converted to radiant intensity in μW/sr by dividing with the solid angle of the sensor. [At one meter the sensor solid angle in sr is essentially the same as its area in square meters.] Then, power measurements were recorded over a wider range of voltages, at small increments, with the sensor placed directly against the display. These readings were scaled to match the one-meter intensities for corresponding voltages. This calibration produced a table of 100 samples from 0.0001 to 70000 μW/sr. Experiment applications used linear interpolations from this table to convert a requested intensity to the necessary LED voltage.

Voltage measurements were taken at one LED within a group to confirm that the number of dots turned on at one time had minimal effect on actual intensity. Turning on 48 dots on a 64-dot module reduced the voltage by less than 3% compared to turning on a single dot.

Oscilloscope traces from a fast photodiode were captured to verify the timing and relative intensity control of ultra-brief flashes. An Advanced Photonix PDB-C156 PIN silicon photodiode was used in unbiased, unamplified photovoltaic mode, with an appropriate load resistor to convert the current output into a voltage that was measured by a 1X voltage probe. Flash intensity was verified by comparing oscilloscope traces for flashing and steady emission.

To account for imperfections in the intensity vs. time shape of brief flash emissions, additional radiometer measurements were taken during periodic flashing at 500Hz and higher – well above the meter analog averaging bandwidth of 30Hz – for a range of flash durations and intensities. These measurements were compared to steady intensity, and an empirical time-dependent compensation formula for the voltage-to-intensity conversion was determined.

The total energy of a flash as seen by a subject, in photons, can be computed as radiant intensity (μW/sr) $\times$ flash duration (μsec) $\times$ 34.26, this being for: wavelength = 633 nm, pupil diameter = 6.66 mm, source distance = 1.8 m.

B. RESEARCH AUTHORIZATION AND INFORMED CONSENT

Experimental protocols were approved by the USC Institutional Review Board. Respondents were recruited from the USC Psychology Subject Pool. Twenty respondents provided judgments for each of the experiment (four males, nineteen females, with age range being 18-23). Each was provided with instructions about the nature of the task, was told that participation was voluntary, and that they could discontinue at any time without penalty. Each completed the experiment without difficulty, and the data from each respondent that was recruited has been included in the statistical analysis.

C. TASK DESIGN AND PROTOCOLS

Discrimination of shape differences can be very sharp, with respondents claiming dissimilarity over minor variations. To counter this issue, pair members were displayed as brief flashes and the second member was displayed at a reduced (12%) density. Also, the instructions provided to respondents included the claim that about half of the trails would be displaying the same shape.

The random sample of 320 pairs was used in a match recognition task wherein respondents were asked to say whether the pair members were the same. Another 40 shapes were chosen from the inventory for display as matching pairs. Judgement of these pairs provided a baseline against which judgments of non-matching pairs could be compared. Each of the 360 pairs was displayed once, the order being determined at random for a given respondent. Each pair member was displayed as a simultaneous flash of all the dots for 10 μs, with 300 ms of separation between the displays. Pair members were displayed in different corners of the board, chosen at random, requiring that at least one dot be in the outermost row and one be in the outermost column, as illustrated in Figure 4.

Between trials the respondent maintained attention on a fixation stimulus that is at the center of the board. Upon launch of the trials the fixation stimulus disappeared, and the pair sequence was displayed. Respondents observed the two shapes and immediately voiced a judgment as to whether the two were the ''Same'' or were ''Different.'' This response was logged into the computer records by a keystroke, which automatically initiated the next trial. Neither the experimenter nor the respondent was provided with information about the pairs being judged.

D. CONSISTENCY OF MATCH JUDGMENTS

Each pair was shown only once to a given respondent, so the decision about a given pair was binary, i.e., scored as a 1 or 0, depending on whether the judgment was ''same'' or ''different,'' respectively. To evaluate whether the judgments were consistent, the mean probability of judgments across all pairs was calculated for a random selection of 10 respondents, and this was compared to the probability for the remaining 10 respondents. This comparison was done separately for the 40 matching pairs, i.e., where the same shape was used

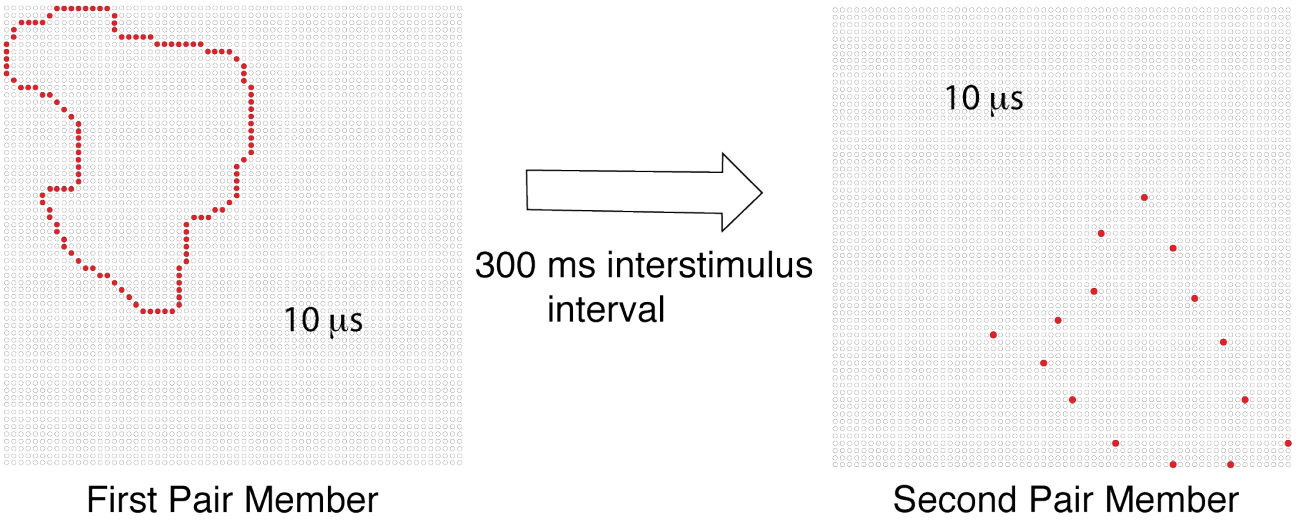

FIGURE 4. The members of a pair were each displayed for 10 μs, with the interval between the two displays being 300 ms. The second member of the pair was shown at a 12% density, and the respondent judged whether the two shapes were the same. The goal here was to determine if the frequency for judging non-matching shapes as being the same was predicted by the size of the similarity values provided by Procrustes analysis or the scan-encoding method.

for both displays, and for the 320 non-matching pairs. This process was repeated 1000 times with random selection of which respondent data would be included in the two groups, and the results of this analysis are shown in Table 1.

TABLE 1. Correlation of match-recognition judgments across respondents.

Correlations	Min	Max	Mean	Median	Std Dev
Matching Pairs	-0.17	0.586	0.099	0.094	0.0037
Non-matching Pairs	0.661	0.791	0.734	0.734	0.0197

Judgments of non-matching pairs were consistent across respondents, as reflected in a high level of correlation of the mean probability of judgments for randomly selected groups of half the respondents compared to the other half. Matching pairs manifested a very low correlation. This outcome likely reflects the fact that all the matching shapes had similarity scores of zero. Further, the overall proportion of "same" judgments was 0.875. Likely any variation for this treatment condition was due to random fluctuation of attention or other judgment factors having little to do with the specific features that each shape provided.

E. PREDICTION OF NON-MATCHING JUDGMENTS BY COMPUTED SIMILARITY VALUES

A major goal of the present work was to determine whether computed shape-similarity measures would predict human judgments of shape similarity. The major relevant data was provided by the 320 non-matching shapes. Valid assessment of whether the pairs were the same should yield consistent judgments that the two displays were different. To the extent that respondents judged non-matching pairs as being the same, they were affirming that the two members were similar to some degree.

The probability of "same" judgments was calculated for the 320 non-matching pairs and the mean for each shape pair was analyzed using binomial regression against the corresponding P-difference values for the pairs, and again against the corresponding S-difference values. The regressions were constrained by requiring that the resulting model be monotonic on the principle that a non-monotonic prediction would not provide a useful index of the perceived similarity of shapes. This restriction yielded models where only the linear regression component was included, though one should note that binomial regression allows some curvature in the model even when it is based only on the linear component.

Figure 5 shows the regression models that were derived for the two computed similarity scales. Clearly the P-difference values did not provide differential prediction of the probability of "same" judgments as a function of the size of the values, whereas the S-difference values provided significant predictions ($p < 0.0001$).

Binomial regressions do not provide a proper way to measure R^2, but one can specify the correlations between the computed similarity scales and the judgment data. The Pearson correlation for the P-difference values was 0.004, and the correlation for S-difference values was 0.40.

IV. DISCUSSION

The values of the Procrustes-similarity scale were completely uncorrelated with those in the scan-similarity scale. The two methods of assessing similarity are clearly registering different characteristics of the shapes. The Procrustes method is not registering any shape attribute other than the spans that separate local markers. In fact, using the smallest net differential between dot pairs as the similarity metric requires that the summary captures only local distance differentials.

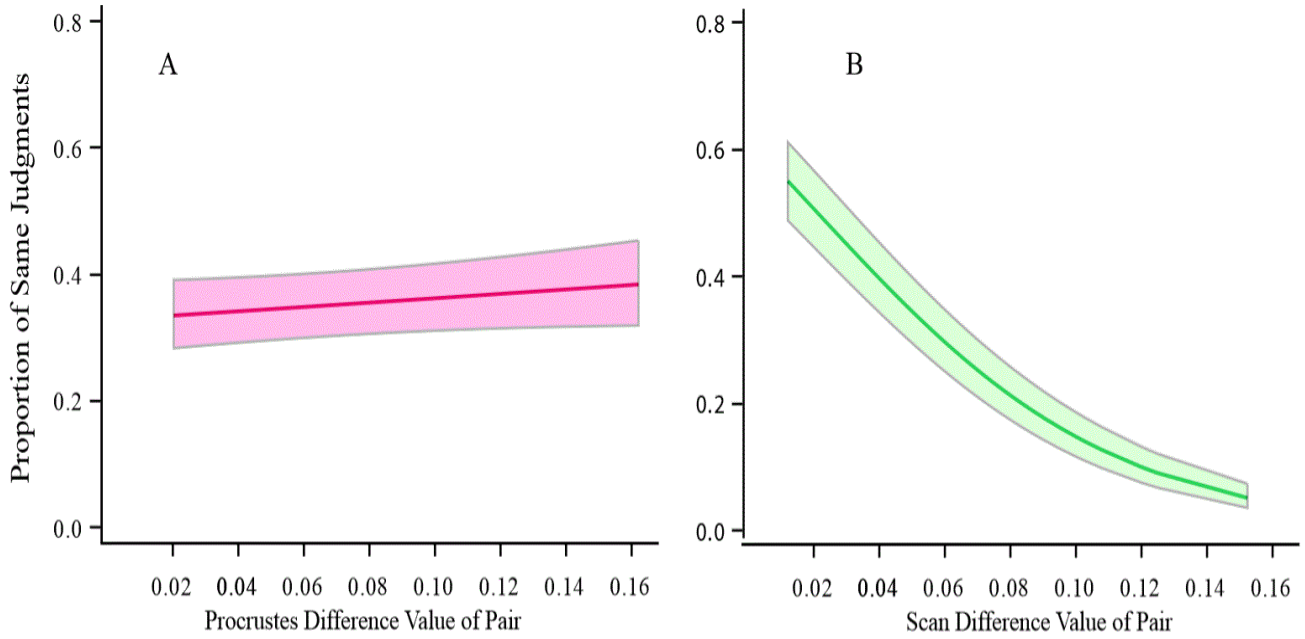

FIGURE 5. A. Procrustes difference values did not predict the proportion of "same" judgments for the non-matching pairs. To the extent that a trend can be seen, the pairs that scored as more different based on the P-difference score were more frequently judged as having the same shape. B. The S-difference scores did predict the probability of "same" judgments. Those with a low difference score were judged as having the same shape for more than half of the pairs, and less than 10% of those with a high difference score were judged as having the same shape.

Procrustes analysis is computationally demanding, so if the scale values had yielded effective prediction of similarity judgments, providing a plausible explanation for how neuronal mechanisms could derive the minimum net distance would have been a major challenge. By comparison, the scan method registers boundary information from markers that are often widely separated, which means that global relationships contribute to the summary. It is interesting that this simple method for summarizing shapes provides some ability to predict human judgments of similarity. This finding may suggest new options for development of neuromorphic image encoding tools.

In recent years a number of laboratories have proposed new concepts for how spatial information is encoded by the retina, some of these having implications for how to register shape boundaries. Gollisch and Meister [41] proposed that retinal ganglion cells are synchronously activated by local contrast features at the end of saccadic eye movements. This would provide a wave of spikes from the array of cells that received a triggering stimulus, such as the boundary of a shape. Rucci and Victor [42] report that visibility of high spatial frequencies is enhanced by the drift that occurs between fixation movements, which argues that small eye motions can contribution to contour detection. Ahissari and Arieli [43] suggest a similar process wherein small drift motions of the eye that occur during ''steady'' fixation can register contours as temporal codes.

Thorpe and associates [44]–[47] have provided evidence of very fast shape recognition that requires new image encoding concepts. They argue against the traditional view that the stimulus information is reflected in neuron firing rates, and propose that the image features are captured and conveyed by the latency of firing of retinal ganglion cells. This ''latency encoding'' concept was presaged by Bullock and associates [48] and was elaborated by Hopfield [49], [50]. The basic concept calls for registering local patterns of brightness differentials in the image, essentially providing filters that detect textures and contours. The hypothesized latency code that is sent forth from the population of retinal ganglion cells would depend on the stimulus pattern.

Several recent studies of retinal physiology support this new approach. There is now clear evidence that the excitatory receptive field of retinal ganglion cells may have a micro-architecture of synaptic influence that registers spatial information within the stimulus. High-contrast spatial frequencies can elicit a complex profile of response that reflects non-linear encoding of the stimuli [51]–[53]. Turner and Rieke [54] examined non-linear responses of parasol ganglion cells of Macaque monkeys in response to naturalistic movies. Their results indicate that the cells are especially activated by the edge elements within the scenes. Onken *et al.* [55] use tensor factorization to evaluate population responses of salamander retina and provide evidence that the first-spike latencies capture information about the spatial contrast relationships.

While we have no objection to the concept that local spatial information, e.g., textures, might be encoded by registering latency of firing within a neuron population, we are concerned about the scale of the supporting data. Discussions of spatiotemporal encoding by the retina appear to have much in common with models of orientation selectivity, wherein the local differentials of light and dark are the critical stimuli.

The present result argues that shape recognition is far more dependent on global positioning of boundary markers than on local stimulus cues. Match recognition was found when the target was at 100% density and the density of the comparison shape was as low as 4% [56], which requires a mechanism for encoding shape properties with large-scale separation of boundary markers. Greene [57], [58] has presented a number of reasons why local contour attributes are not essential for shape recognition. The boundary markers do not make their locations known using coordinate addresses, but a polling mechanism might provide a way to transcribe that information. On balance, we are positive about the use of a population code, perhaps one that focuses on a wave of first spikes, and we favor the concept that a polling mechanism is used to elicit the spikes from marked boundary locations.

V. NEUROMORPHIC RELEVANCE

Returning to the issue of neuromorphic implementation, many have used electronic circuits to detect motion and mark contours in an image. The silicon retina developed by Mahowald and Mead [59] registers the contours of a moving object. Two-dimensional sheets of e-neurons provide so-called ''excitable membranes'' that can detect motion [60], register motion speed [61], or mark the contours of gray-scale images [62]–[65]. The Rasche design [65] uses spreading waves of subthreshold spikes that selectively activate high-contrast differentials. This kind of global contour-marking mechanism could be an essential first step toward encoding the spatial relations among the marked boundary locations.

Far less effort has be directed toward summarizing the shape information. Tara Hamilton and associates describe an unconventional method for connecting elements of a hexagonal array of sensors that provides for effective encoding of shape contours [66]. They implement a process that polls successive concentric locations on the array, sending a signal from those elements that have registered a portion of the contour. The polling wave passes from the outer ring to the inner one, generating a pulse if a contour-marked element is encountered. This temporal coding concept is essentially a count of the number of markers within each ring. Whereas the scan method described in the present work used horizontal and vertical scans, the Hamilton method [66] scans concentric rings. Both methods provide a one-dimensional shape summary wherein contour markers are counted through polling, with the number of markers encountered at any given moment provide a signal that can be formally represented as height of a histogram bin.

Several alternative polling methods might be needed to achieve effective shape encoding, each providing a different benefit. But even if several were required, the speed and efficiency would be substantially greater than for current computational methods. Hamilton and associates [66] make the point that the encoding done with such ''miniscule nervous systems'' would be useful for autonomous imaging sensor networks, wireless phones, and other embedded vision systems that must deal with problems of limited size, power, and real-time operations. We agree.

ACKNOWLEDGMENT

Respondents were tested by Andrew Geoly, Yash Patel, and Taylor Burchfield.

REFERENCES

[1] P. Ren, B. Chen, Z. Yuan, and N. Zheng, ''Toward robust visual cognition through brain-inspired computing,'' in *Brain-Inspired Intelligent Robotics: The Intersection of Robotics and Neuroscience*. 2016, p. 16.
[2] B. Zhang, L. P. Shi, and S. Song, ''Creating more intelligent robots through brain-inspired computing,'' in *Brain-Inspired Intelligent Robotics: The Intersection of Robotics and Neuroscience*. 2016, pp. 4–9.
[3] K. Fukushima, ''Neocognitron: A self-organizing neural network model for a mechanism of pattern recognition unaffected by shift in position,'' *Biol. Cybern.*, vol. 36, no. 4, pp. 193–202, 1980.
[4] E. T. Rolls, A. Cowey, and V. Bruce, ''Neurophysiological mechanisms underlying face processing within and beyond the temporal cortical visual areas,'' *Philos. Trans., Biol. Sci.*, vol. 335, no. 1273, pp. 11–21, 1992.
[5] G. Wallis and E. T. Rolls, ''Invariant face and object recognition in the visual system,'' *Prog. Neurobiol.*, vol. 51, no. 2, pp. 167–194, Feb. 1997.
[6] A. J. Rodriguez-Sánchez and J. K. Tsotsos, ''The roles of endstopped and curvature tuned computations in a hierarchical representation of 2D shape,'' *PLoS ONE*, vol. 7, no. 8, p. e42058, 2012.
[7] M. Riesenhuber and T. Poggio, ''Models of object recognition,'' *Nature Neurosci. Suppl.*, vol. 3, pp. 1199–1204, Nov. 2000.
[8] A. Pasupathy and C. E. Connor, ''Shape representation in area V4: Position-specific tuning for boundary conformation,'' *J. Neurophysiol.*, vol. 86, pp. 2505–2519, Nov. 2001.
[9] N. Suzuki, N. Hashimoto, Y. Kashimori, M. Zheng, and T. Kambara, ''A neural model of predictive recognition in form pathway of visual cortex,'' *Biosystems*, vol. 76, nos. 1–3, pp. 33–42, Aug./Oct. 2004.
[10] N. Pinto, D. D. Cox, and J. J. DiCarlo, ''Why is real-world visual object recognition hard?'' *PLoS Comput. Biol.*, vol. 4, p. e27, Jan. 2008.
[11] Y. LeCun, Y. Bengio, and G. Hinton, ''Deep learning,'' *Nature*, vol. 521, pp. 436–444, May 2015.
[12] I. Karplus, M. Goren, and D. Algom, ''A preliminary experimental analysis of predator face recognition by *Chromis caeruleus* (Pisces, Pomacentridae),'' *Zeitschrift Tierpsychol.*, vol. 58, no. 1, pp. 53–65, 1982.
[13] U. E. Siebeck, A. N. Parker, D. Sprenger, L. M. Mäthger, and G. Wallis, ''A species of reef fish that uses ultraviolet patterns for covert face recognition,'' *Current Biol.*, vol. 20, no. 5, pp. 407–410, 2010.
[14] I. Karplus, R. Katzenstein, and M. Goren, ''Predator recognition and social facilitation of predator avoidance in coral reef fish *Dascyllus marginatus* juveniles,'' *Mar. Ecol. Prog. Ser.*, vol. 319, pp. 215–223, Aug. 2006.
[15] U. E. Siebeck, L. Litherland, and G. M. Wallis, ''Shape learning and discrimination in reef fish,'' *J. Exp. Biol.*, vol. 212, no. 13, pp. 2113–2119, 2009.
[16] C. Newport, G. Wallis, Y. Reshitnyk, and U. E. Siebeck, ''Discrimination of human faces by archerfish (*Toxotes chatareus*),'' *Sci. Rep.*, vol. 6, p. e27523, Jun. 2016.
[17] F. Abbas and M. P. Martin, ''Fish vision: Size selectivity in the zebrafish retinotectal pathway,'' *Current Biol.*, vol. 24, no. 21, pp. 1048–1050, 2014.
[18] E. Greene and M. J. Hautus, ''Demonstrating invariance encoding of shapes using a matching judgment protocol,'' *AIMS Neurosci.*, vol. 4, no. 3, pp. 120–147, 2016.
[19] E. Greene and Y. Patel, ''Scan transcription of two-dimensional shapes as an alternative neuromorphic concept,'' *Trends Artif. Intell.*, vol. 1, pp. 27–33, Mar. 2018.
[20] D. G. Kandell, ''The statistics of shape,'' in *Interpreting Multivariate Data*, V. Barnett, Ed. New York, NY, USA: Wiley, 1981, pp. 75–80.
[21] D. G. Kendall, ''Shape manifolds, procrustean metrics, and complex projective spaces,'' *Bull. Lond. Math. Soc.*, vol. 16, no. 2, pp. 81–121, Mar. 1984.
[22] D. G. Kendall, ''Exact distributions for shapes of random triangles in convex sets,'' *Adv. Appl. Probab.*, vol. 17, no. 2, pp. 308–329, 1985.
[23] C. Goodall, ''Procrustes methods in the statistical analysis of shape,'' *J. Roy. Statist. Soc.*, vol. 53, no. 2, pp. 285–339, 1991.
[24] E. del Castillo, ''Statistical shape analysis of manufacturing data,'' in *Geometric Tolerances: Impact on Product Design, Quality Inspection and Statistical Process Monitoring*, B. Colosimo and N. Senin, Eds. New York, NY, USA: Springer, 2011, pp. 215–234.

[25] F. L. Bookstein, "Random walk as a null model for high-dimensional morphometrics of fossil series: Geometrical considerations," *Paleobiology*, vol. 39, no. 1, pp. 52–74, 2012.
[26] P. Vermeesch and E. Garzanti, "Making geological sense of 'big data' in sedimentary provenance analysis," *Chem. Geol.*, vol. 409, pp. 20–27, Aug. 2015.
[27] P. Mitteroecker, P. Gunz, S. Windhager, and K. Schaefer, "A brief review of shape, form, and allometry in geometric morphometrics, with applications to human facial morphology," *Hystrix, Italian J. Mammal.*, vol. 24, no. 1, pp. 59–66, 2013.
[28] D. C. Adams, F. J. Rohlf, and D. E. Slice, "Geometric morphometrics: Ten years of progress following the 'revolution,'" *Italian J. Zool.*, vol. 71, no. 1, pp. 5–16, 2004.
[29] P. O'Higgins, "The study of morphological variation in the hominid fossil record: Biology, landmarks and geometry," *J. Anatomy*, vol. 197, no. 1, pp. 120–203, 2000.
[30] D. E. Slice, "Modern morphometrics," in *Modern Morphometrics in Physical Anthropology*, D. E. Slice, Ed. New York, NY, USA: Klewer, 2005, pp. 1–45.
[31] D. E. Slice, "Geometric morphometrics," *Ann. Rev. Anthropol.*, vol. 36, pp. 261–281, Oct. 2007.
[32] P. Mitteroecker and P. Gunz, "Advances in geometric morphometrics," *Evol. Biol.*, vol. 36, no. 2, pp. 235–247, Jun. 2009.
[33] D. C. Adams, F. J. Rohlf, and D. E. Slice, "A field comes of age: Geometric morphometrics in the 21st century," *Hystrix, Italian J. Mammal.*, vol. 24, no. 1, pp. 7–14, 2013.
[34] I. L. Dryden and K. V. Mardia, *Statistical Shape Analysis*, 2nd ed. London, U.K.: Wiley, 2016.
[35] L. Cangiano, S. Asteriti, L. Cervetto, and C. Gargini, "The photovoltage of rods and cones in the dark-adapted mouse retina," *J. Physiol.*, vol. 590, no. 16, pp. 3841–3855, 2012.
[36] L.-H. Cao, D.-G. Guo, and K.-W. Yau, "Light responses of primate and other mammalian cones," *Proc. Nat. Acad. Sci. USA*, vol. 111, no. 7, pp. 2752–2757, 2014.
[37] G. D. Field *et al.*, "High-sensitivity rod photoreceptor input to the blue-yellow color opponent pathway in macaque retina," *Nature Neurosci.*, vol. 12, pp. 1159–1164, Aug. 2009.
[38] O. S. Packer, D. R. Williams, and D. G. Bensinger, "Photopigment transmittance imaging of the primate photoreceptor mosaic," *J. Neurosci.*, vol. 16, no. 7, pp. 2251–2260, 1996.
[39] J. L. Schnapf, B. J. Nunn, M. Meister, and D. A. Baylor, "Visual transduction in cones of the monkey Macaca fascicularis," *J. Physiol.*, vol. 427, no. 1, pp. 681–713, 1990.
[40] D. M. Schneeweis and J. L. Schnapf, "The photovoltage of macaque cone photoreceptors: Adaptation, noise, and kinetics," *J. Neurosci.*, vol. 19, no. 4, pp. 1203–1216, 1999.
[41] T. Gollisch and M. Meister, "Rapid neural coding in the retina with relative spike latencies," *Science*, vol. 319, no. 5866, pp. 1108–1111, Feb. 2008.
[42] M. Rucci and J. D. Victor, "The unsteady eye: An information-processing stage, not a bug," *Trends Neurosci.*, vol. 38, no. 4, pp. 195–206, 2015.
[43] E. Ahissar and A. Arieli, "Seeing via miniature eye movements: A dynamic hypothesis for vision," *Frontiers Comput. Neurosci.*, vol. 6, pp. 1–27, Nov. 2012.
[44] S. J. Thorpe, D. Fize, and C. Marlot, "Speed of processing in the human visual system," *Nature*, vol. 381, no. 6582, pp. 520–522, 1996.
[45] R. VanRullen and S. J. Thorpe, "Is it a bird? Is it a plane? Ultra-rapid visual categorisation of natural and artifactual objects," *Perception*, vol. 30, pp. 655–668, Jun. 2001.
[46] R. VanRullen and S. J. Thorpe, "Surfing a spike wave down the ventral stream," *Vis. Res.*, vol. 42, no. 23, pp. 2593–2615, 2002.
[47] H. Kirchner and S. J. Thorpe, "Ultra-rapid object detection with saccadic eye movements: Visual processing speed revisited," *Vis. Res.*, vol. 46, no. 11, pp. 1762–1776, 2006.
[48] T. H. Bullock, S. Karmürsel, and M. H. Hofmann, "Interval-specific event related potentials to omitted stimuli in the electrosensory pathway in elasmobranchs: An elementary form of expectation," *J. Comput. Physiol.*, vol. 172, no. 4, pp. 501–510, 1993.
[49] J. J. Hopfield, "Pattern recognition computation using action potential timing for stimulus representation," *Nature*, vol. 376, no. 6535, pp. 33–36, 1995.
[50] J. J. Hopfield, "Transforming neural computations and representing time," *Proc. Nat. Acad. Sci. USA*, vol. 93, no. 26, pp. 15440–15444, 1996.
[51] E.-C. Christina and J. G. Robson, "The contrast sensitivity of retinal ganglion cells of the cat," *J. Physiol.*, vol. 187, no. 3, pp. 517–552, Dec. 1966.
[52] S. Hochstein and R. M. Shapley, "Linear and nonlinear spatial subunits in Y cat retinal ganglion cells," *J. Physiol.*, vol. 262, no. 2, pp. 265–284, Nov. 1976.
[53] S. Hochstein and R. M. Shapley, "Quantitative analysis of retinal ganglion cell classifications," *J. Physiol.*, vol. 262, no. 2, pp. 237–264, Nov. 1976.
[54] M. H. Turner and F. Rieke, "Synaptic rectification controls nonlinear spatial integration of natural visual inputs," *Neuron*, vol. 90, no. 6, pp. 1257–1271, 2016.
[55] A. Onken, J. K. Liu, P. P. C. R. Karunasekara, I. Delis, T. Gollisch, and S. Panzeri, "Using matrix and tensor factorizations for the single-trial analysis of population spike trains," *PLOS Comput. Biol.*, vol. 12, no. 11, p. e1005189, 2016.
[56] H. Nordberg, M. J. Hautus, and E. Greene, "Visual encoding of partial unknown shape boundaries," *AIMS Neurosci.*, vol. 5, no. 2, pp. 132–147, 2018.
[57] E. Greene, "Rapid de novo shape encoding: A challenge to connectionist modeling," *JSM Brain Sci.*, vol. 3, no. 1, p. e1016, 2018.
[58] E. Greene, "New encoding concepts for shape recognition are needed," *AIMS Neurosci.* vol. 5, no. 3, pp. 162–178, 2018.
[59] M. A. Mahowald and C. Mead, "The silicon retina," *Sci. Amer.*, vol. 264, no. 5, pp. 76–83, 1991.
[60] D. A. Glaser and D. Barch, "Motion detection and characterization by an excitable membrane: The 'bow wave' model," *Neurocomputer*, vols. 26–27, pp. 137–146, Jun. 1999.
[61] C. Rasche, "Speed estimation with propagation maps," *Neurocomputing*, vol. 69, nos. 13–15, pp. 1599–1607, Aug. 2005.
[62] C. Rasche, "Signaling contours by neuromorphic wave propagation," *Biol. Cybern.*, vol. 90, no. 4, pp. 272–279, 2004.
[63] C. Rasche, "A neural architecture for the symmetric-axis transform," *Neurocomputing*, vol. 64, pp. 301–317, Mar. 2005.
[64] C. Rasche, *The Making of a Neuromorphic Visual System*. New York, NY, USA: Springer-Verlag, 2005.
[65] C. Rasche, "Neuromorphic excitable maps for visual processing," *IEEE Trans. Neural Netw.*, vol. 18, no. 2, pp. 520–529, Mar. 2007.
[66] S. Afshar *et al.*, "The ripple pond: Enabling spiking networks to see," *Frontiers Neurosci.*, vol. 7, p. e212, Nov. 2013.

ERNEST GREENE received the Ph.D. degree in behavioral neuroscience from the University of Oregon in 1968. He was a Post-Doctoral Fellow with the Brain Research Institute, UCLA, before joining the Faculty at the University of Southern California (USC). He is currently a Professor of psychology with USC and also the Head of the Laboratory for Neurometric Research. His honors include election to the National Academy of Neuropsychology, a Charter Fellow of the Association for Psychological Science, and a fellow of the American Association for the Advancement of Science. He has three patents and has published journal articles in fields that include behavioral neuroscience, clinical neuropsychology, psychophysics, cognitive neuroscience, and artificial intelligence. Recent work has focused on visual illusion mechanisms, persistence of visual information, and shape recognition mechanisms.

JACK MORRISON received the B.S. degree in computer science from UCLA. His engineering experience includes software and electronics development for a wide variety of commercial, research, and spaceflight projects. He currently runs a consulting business Digital Insight, focused on embedded systems and robotics. He has co-authored journal articles on space robotics. He received a NASA Public Service Medal for the autonomous design of the Sojourner Mars rover.